ARTICLE IN PRESS

Available online at www.sciencedirect.com
SCIENCE DIRECT®

Surface Science xxx (2006) xxx–xxx

SURFACE SCIENCE

www.elsevier.com/locate/susc

The morphology and nucleation kinetics of copper islands during electrodeposition

A. Radisic [a], P.M. Vereecken [b], P.C. Searson [a,*], F.M. Ross [b,*]

[a] *Department of Materials Science and Engineering, Johns Hopkins University, 3400 N Charles St. Baltimore, MD 21218, United States*
[b] *IBM T. J. Watson Research Center, 1101 Kitchawan Road, Yorktown Heights, NY 10598, United States*

Received 7 November 2005; accepted for publication 8 February 2006

Abstract

We describe a study, using in situ transmission electron microscopy, of the shape and nucleation kinetics of three-dimensional islands formed during the electrochemical deposition of copper. By operating an electrochemical cell within an electron microscope, we obtain real-time images of the formation of copper islands on a gold electrode while simultaneously recording electrochemical data such as voltage and current. We first present cyclic voltammetry, where the images show the deposition and stripping processes while the voltammogram demonstrates qualitatively the regimes in which diffusion and surface reaction are the rate limiting steps. We then examine island growth quantitatively under conditions of constant potential. Images recorded during growth at various potentials allow direct visualization of the differences between island shapes in the diffusion limited and kinetically limited growth regimes. Furthermore, a combined analysis of the current transients and the images allows parameters such as the diffusion coefficient, the rate constant and the critical nucleus size to be determined. We discuss these results in the context of electrochemical nucleation and growth models.

Keywords: Island growth; Transmission electron microscopy; Copper; Electrodeposition

1. Introduction

Studies of electrochemical nucleation and growth are commonly performed by comparing the data obtained using macroscopic electrochemical measurements and ex situ imaging techniques to the rate laws available in the literature [1–7]. These studies sometimes lead to conclusions that are difficult to explain with tools currently available. For example, for the deposition of copper on TiN from pyrophosphate solution [4–6], current–time transients are consistent with rate laws which assume instantaneous nucleation followed by diffusion limited growth of three-dimensional (3-D) islands [8,9]. Yet observations of the islands that actually grow show densities several orders of magnitude higher than those predicted by fitting the rate laws to the current–time data.

Part of the difficulty in analyzing such experimental data is that analytical solutions for electrochemical nucleation and growth are derived for a small number of limiting cases, using simplifying approximations. For example, in the models for instantaneous and progressive nucleation followed by 3-D diffusion limited growth [8,9], it is assumed that deposition occurs exclusively through direct attachment of ions to growing nuclei. In many cases, electrochemical systems are more complicated. Copper plating baths usually contain additives such as levelers and brighteners [10–12], and processes such as adsorption and surface diffusion can take place at the same time as ions are directly attaching to the growing islands. Another problem is that images obtained using ex situ techniques such as scanning electron microscopy (SEM) and atomic force microscopy (AFM) contain information on the distribution of islands only at one particular time. The time evolution of the

* Corresponding authors.
E-mail addresses: searson@jhu.edu (P.C. Searson), fmross@us.ibm.com (F.M. Ross).

0039-6028/$ - see front matter © 2006 Elsevier B.V. All rights reserved.
doi:10.1016/j.susc.2006.02.025

island density can be obtained by performing many experiments at different deposition times, but this approach is extremely time consuming.

In this paper we report on simultaneous in situ, real-time, high resolution imaging of copper deposition on gold in conjunction with electrochemical measurements. These experiments were carried out by operating a small, vacuum-compatible, three-electrode electrochemical cell within a transmission electron microscope (TEM). By carrying out electrochemical deposition in an electron transparent layer of electrolyte, it is possible to obtain video-rate (30 frames per second) TEM images of the growth of clusters, simultaneously with measurements of the voltage applied to the cell and the current flowing through it. In this paper, we analyze island structure and nucleation kinetics based on this real-time data.

We first show images recorded simultaneously with current–voltage curves. These data verify the operation of the electrochemical cell, show the deposition and stripping processes directly, and demonstrate qualitatively the regimes in which diffusion and surface reaction are expected to be the rate limiting steps. We then describe island growth at constant potential. Sequences of images recorded at different potentials allow a direct visualization of the changes in island morphology for the diffusion limited and kinetically limited growth regimes. A combined analysis of the current transients and the images then allows key growth parameters to be determined. The results of this analysis are significant when considered in the context of electrochemical nucleation and growth models which were originally developed based only on macroscopic measurements such as current transients. Our results verify directly one key assumption of nucleation and growth models that nucleation kinetics are first order, and provide values for the rate constant and the nucleus density as a function of potential. These lead to a value for the critical nucleus size that is in agreement with the value derived from other techniques. The combination of real-time imaging and electrochemical measurements therefore provide a quantitative basis for testing and improving electrochemical nucleation and growth models.

2. Experimental

The thin layer cell used for in situ, real-time TEM imaging of electrochemical deposition is shown schematically in Fig. 1. This cell is based on an earlier, two terminal design that was used to investigate electrodeposition under conditions of constant current [13]. Since more complete information can be obtained in a three electrode arrangement, the design was modified to include a reference electrode. Further modifications improved the reliability of the cell, and the cell's overall design and initial results are described elsewhere [14,15]. Briefly, the cell was fabricated from two silicon wafers coated with a 100 nm thick SiN layer, with each wafer etched to create a 100×100 μm SiN viewing window that is transparent for the energetic electrons used

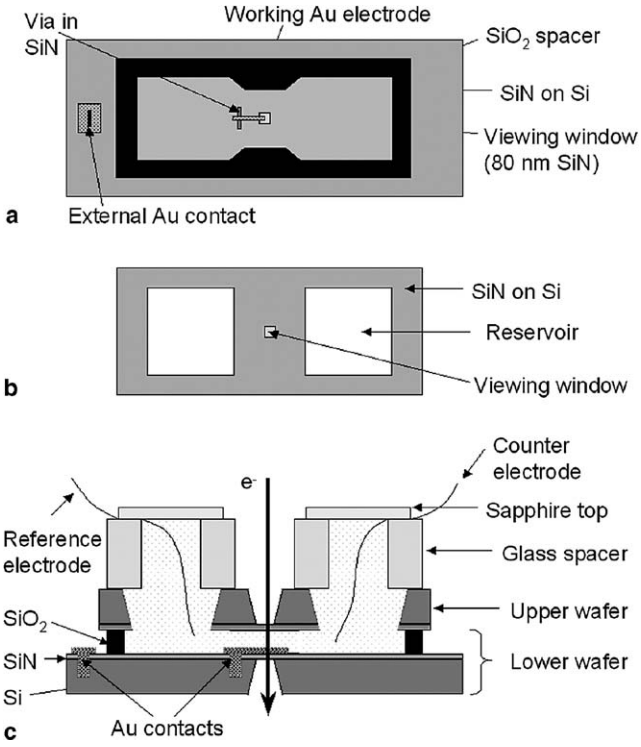

Fig. 1. Schematic of the TEM liquid cell: (a) lower wafer, (b) upper wafer, and (c) cross-section of the assembled cell.

for imaging [13]. In the present experiments, the working electrode was fabricated by evaporating 20 nm gold on a 5 nm Ti adhesion layer onto the SiN window of the lower wafer and over a via, thereby creating a connection through the wafer, which was highly doped, to an external contact. The evaporated gold film had a (1 1 1) texture and a grain size of about 10 nm. The total area of the working electrode was 2×10^{-5} cm^2. To increase the total volume of electrolyte in the cell and allow for better contact with the other two electrodes, two openings (0.04 cm^2) on either side of the viewing window were etched through the entire upper wafer and glass washers attached to the openings to serve as reservoirs. Prior to assembling a cell, the wafers were rinsed sequentially with acetone, ethanol, and doubly deionized water. The wafers were then immersed in 10% HNO_3 for several minutes before a final rinse in doubly deionized water. The reference electrode (a copper wire) and the counter electrode (a gold wire) were then placed in the reservoirs and electrolyte added using a syringe. Solution from the reservoirs flowed into the volume between the two wafers by capillary action. All experiments were performed in 0.1 M $CuSO_4 \cdot 5H_2O$ (Baker) with 1 vol.% H_2SO_4 (Baker) at pH $\approx$ 1.

After assembling and sealing a cell, voltammograms were recorded to verify that the deposition and stripping features seen in large area cell could be reproduced. The cell was then loaded into a specially designed TEM sample holder with electrical connections for the three electrodes. The cell was initially tested in a small chamber, separated

from the main column of the TEM, equipped with a viewing window and a pressure gauge. Any leaks in the cell resulted in evaporation of the solution and an increase in pressure and could be observed easily. Cells with good seals were then loaded into the microscope column and connected to the potentiostat. The microscope used was a Hitachi H-9000 operating at 300 kV.

3. Copper deposition and dissolution during cyclic voltammetry

Fig. 2 shows cyclic voltammograms recorded in a sealed cell in the TEM column during imaging. The features visible in this voltammogram are in good agreement with those expected for conventional electrochemical cells having large area electrodes and larger volumes of electrolyte. It can be seen that the onset of copper deposition occurs at -0.04 V followed by a current peak of 3.2×10^{-7} A ($16\ \mathrm{mA\ cm^{-2}}$) at -0.11 V, characteristic of diffusion limited island growth. The small current from 0.1 to -0.04 V is not related to electrochemical processes and is ascribed to an uncompensated resistance in the cell. On the reverse scan, the diffusion limited deposition current is about 1×10^{-7} A ($5\ \mathrm{mA\ cm^{-2}}$). Deposition continues to about 0 V, at which point we see the onset of copper dissolution, and a stripping peak is observed at 0.11 V. From the ratio of the oxidation (stripping) and reduction charge we determine an average deposition efficiency of 0.83, indicating that most of the reduction current during the scan is associated with reduction of Cu(II) to Cu(0). Subsequent scans show excellent reproducibility, as shown in Fig. 2.

Fig. 3 shows a series of images recorded simultaneously with the second cycle of the voltammogram, illustrating the evolution of surface morphology during copper deposition. There is no change in the gold surface as the potential is decreased to -0.02 V (Fig. 3(a)). At -0.04 V, corresponding to the onset of copper deposition in the voltammogram, copper islands become visible (Fig. 3(b)). At more negative potentials, the islands continue to grow and more islands appear (Fig. 3(c) and (d)). Close to the potential of the current peak at about -0.095 V, the average radius of the copper islands is about 100 nm (Fig. 3(e)), where the island radius is defined as the radius of a circle having the same area as the projected island area.

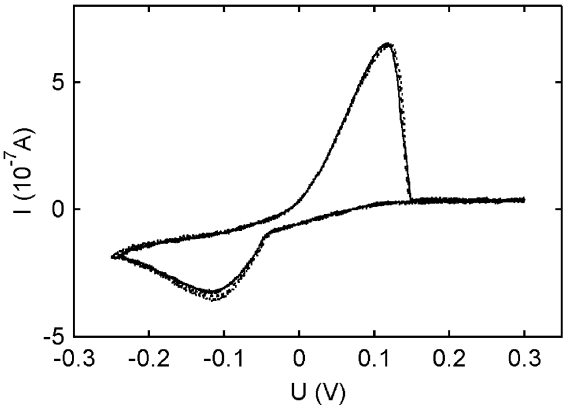

Fig. 2. Cyclic voltammograms for gold in 0.1 M $CuSO_4 \cdot 5H_2O + 1$ vol.% H_2SO_4 in a fully assembled TEM cell in the TEM column recorded at $25\ \mathrm{mV\ s^{-1}}$. Three cycles are shown illustrating the reproducibility of the system.

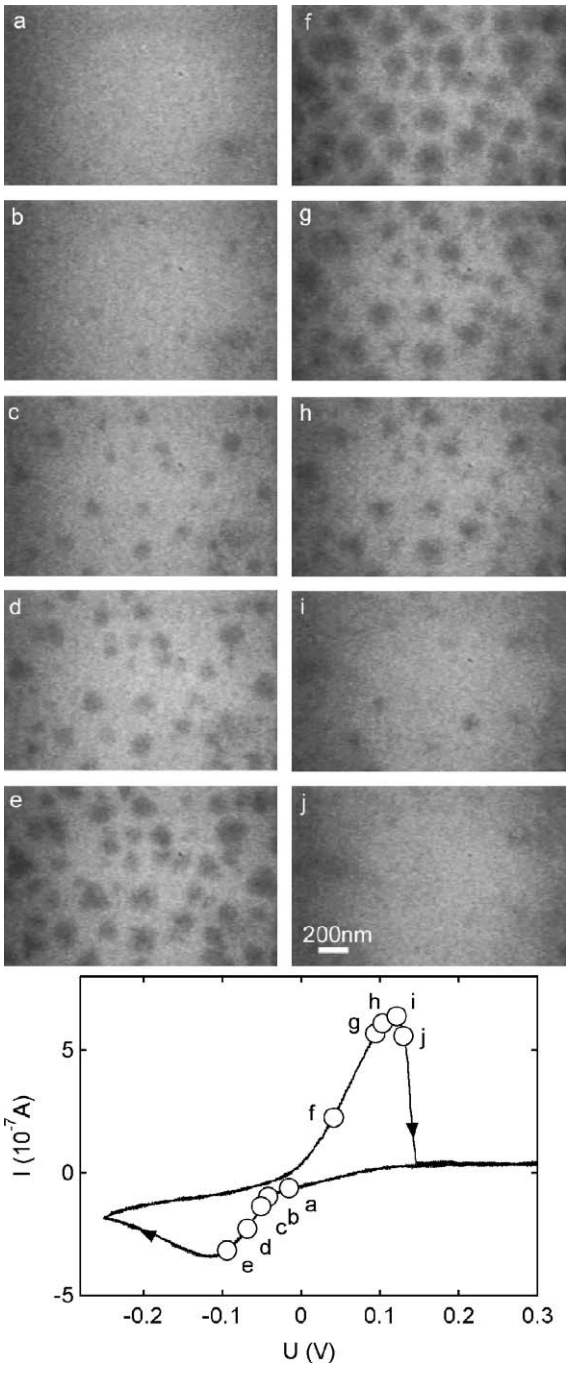

Fig. 3. A sequence of images recorded simultaneously with the second cyclic voltammogram in Fig. 2: (a)–(e) deposition, (f)–(j) stripping. The cyclic voltammogram shows the point in the cycle at which each image was recorded.

The stripping process is illustrated by the series of images shown in Fig. 3(f)–(j). As the potential increases from 0.095 V (Fig. 3(g)) to 0.122 V (Fig. 3(i)) the island density and island radii decrease dramatically. At 0.13 V (Fig. 3(j)) the islands are almost completely dissolved and the current rapidly falls to zero. Images recorded on subsequent cycles showed the same features. It is interesting to note that, in common with island formation at constant current [13], the nucleation sites are different on each cycle, showing that there is not a low density of preferred nucleation sites.

Due to the varying potential applied during cyclic voltammetry, it is difficult to perform quantitative analysis on data of the sort presented above. However, the voltammogram does show important qualitative features of the system. In particular, we see the nucleation, growth, and coalescence of 3-D islands at negative potentials and island dissolution at positive potentials. At small overpotentials close to the onset of deposition, the current increases approximately exponentially with potential, characteristic of kinetically limited growth. At more negative potentials (≈ -0.05 V to -0.1 V), the current increases more slowly due to the depletion of ions at the growing nuclei; this regime is characteristic of mixed kinetic/diffusion control. Finally, at more negative potentials beginning at about the current peak, growth becomes diffusion limited and is controlled by the supply of ions to the growing nuclei. The cyclic voltammogram therefore provides a baseline for analysis of island growth at constant potential, to be discussed below.

4. Deposition at constant potential

4.1. Analysis of current transients

The nucleation kinetics of copper islands on gold were determined by carrying out deposition at constant potential and analyzing the time dependence of the deposition current. In these experiments the potential is first stepped from the open circuit potential ($\approx$0.04 V) to 0.15 V for 2 s to ensure that there is no copper on the gold surface. The potential is then stepped to a value where deposition occurs. Fig. 4(a) shows current–time transients for deposition potentials in the range -0.05 V to -0.1 V. In these curves, the deposition current first increases due to nucleation and 3-D diffusion limited growth of hemispherical copper islands. At longer times the diffusion fields associated with individual islands start interacting and the current decreases, resulting in a transition to 1-D diffusion limited growth. These features are similar to those of current transients obtained for copper deposition on different substrates from various alkaline and acidic solutions [1–7].

At long times, where the diffusion fields are expected to be 1-D (planar), we would expect the current to decay as $t^{-1/2}$, according to the Cottrell equation [16]:

$$I = \frac{zFAD^{1/2}c}{\pi^{1/2}t^{1/2}} \quad (1)$$

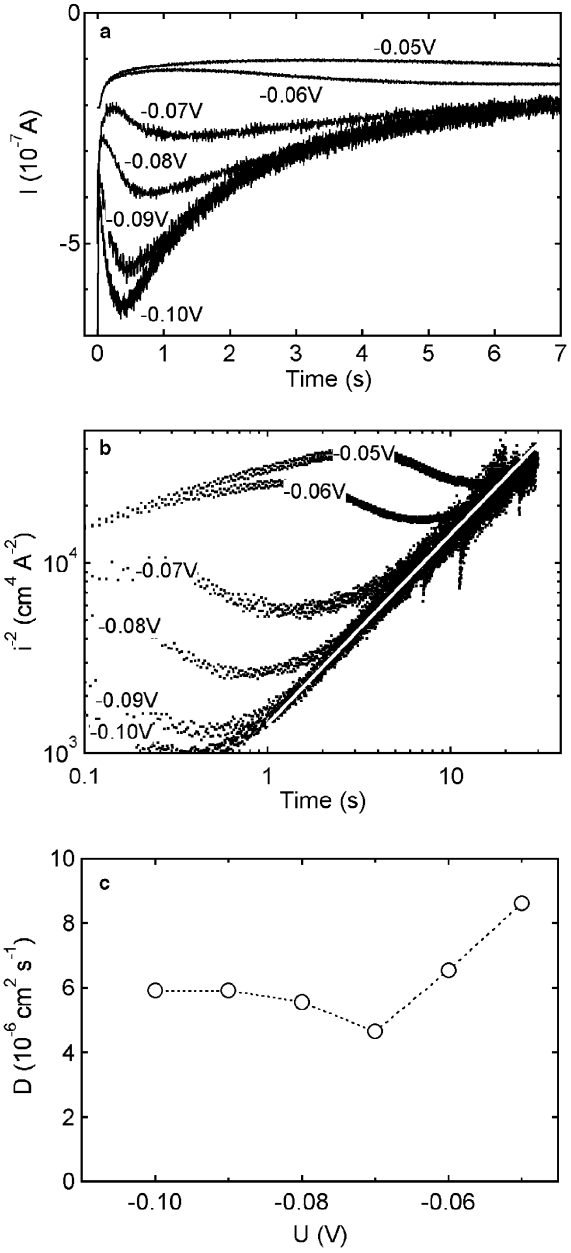

Fig. 4. (a) Current–time transients for deposition at potentials from -0.05 V to -0.10 V. (b) $\log i^{-2}$ versus $\log t$ plots of the deposition transients. The solid line corresponds to the Cottrell equation with $D = 6 \times 10^{-5}$ cm^2 s^{-1}. (c) Potential dependence of the diffusion coefficient for copper ions in the bulk solution calculated from the slopes of the i^{-2} versus t plots in (b).

where z is the charge on the ion, F is Faraday's constant, A is the electrode area, c is the bulk concentration of ions, and D is the diffusion coefficient. Fig. 4(b) shows the current–time curves replotted as $\log i^{-2}$ versus $\log t$. The linear dependence seen at long times (long compared to t_{max}) suggests that growth is indeed controlled by planar diffusion of ions to the islands. From Eq. (1), the diffusion coefficient can be calculated and results are shown in Fig. 4(c). For the most negative potentials, we find that the diffusion coefficient approaches 6×10^{-6} cm^2 s^{-1}, in excellent agreement

with the bulk value reported in the literature [17]. However, the apparent value obtained at more positive potentials, where Fig. 2 suggests that deposition is under mixed kinetic/diffusion control, deviates significantly from the bulk value. From Fig. 4(c) we can see that the transition between diffusion control and mixed control occurs at about −0.07 V.

4.2. Analysis of images

Figs. 5–10 show a series of images extracted from videos recorded simultaneously with the current transients we have just presented. In Fig. 5, deposition was carried out at −0.05 V. At this low overpotential, deposition is under mixed diffusion/kinetic control. The rate of island formation is very slow and for the first seven seconds there is no evidence of deposition. After this time, a single island becomes visible in the field of view. The island is faceted, indicating that surface diffusion plays a significant role in influencing island morphology. At more positive deposition potentials the rate of surface diffusion is expected to be fast in comparison to the rate at which metal ions are reduced to metal atoms at the surface, resulting in the formation of facets on the islands. The effective radius of the island increases with time, and we observe changes in contrast going from the edge toward the center of the island, suggesting that the island shape is close to a three-sided pyramid.

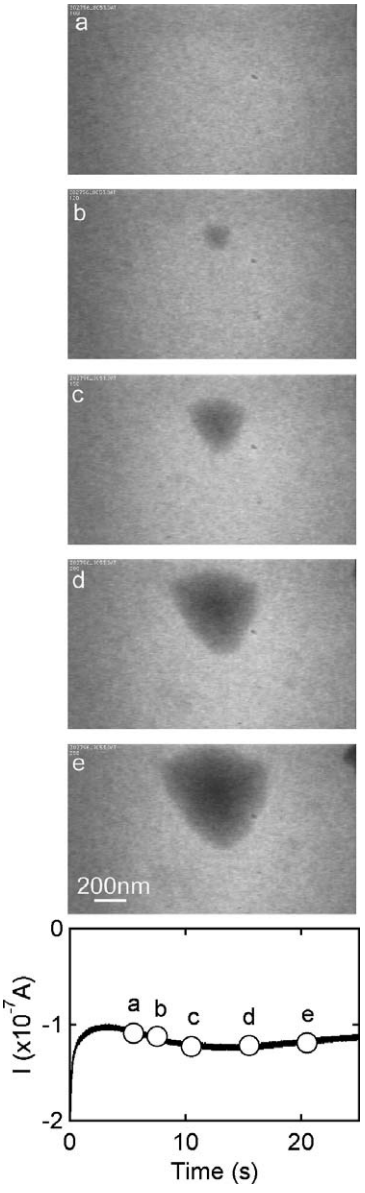

Fig. 5. A sequence of images recorded simultaneously with deposition at −0.05 V. The current transient curve below shows the time at which each image was recorded.

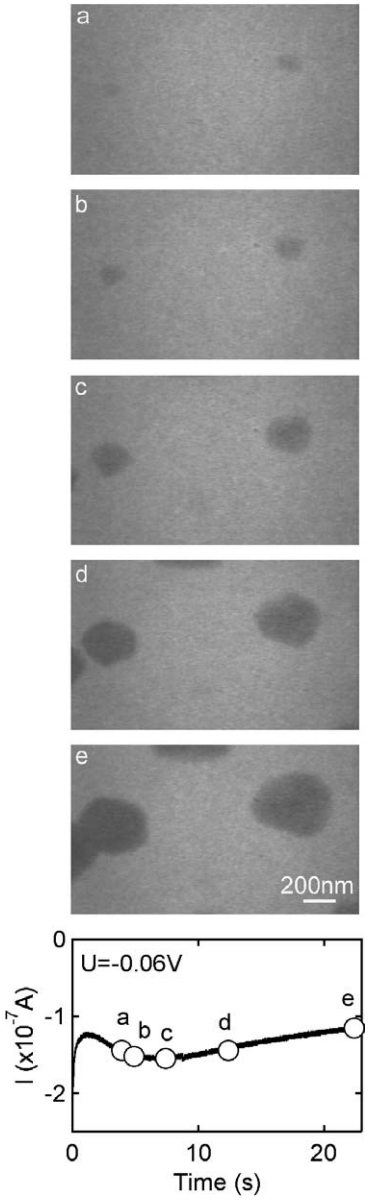

Fig. 6. A sequence of images recorded simultaneously with deposition at −0.06 V.

Fig. 6 shows a series of frames recorded during deposition at −0.06 V. Two islands are seen in the field of view

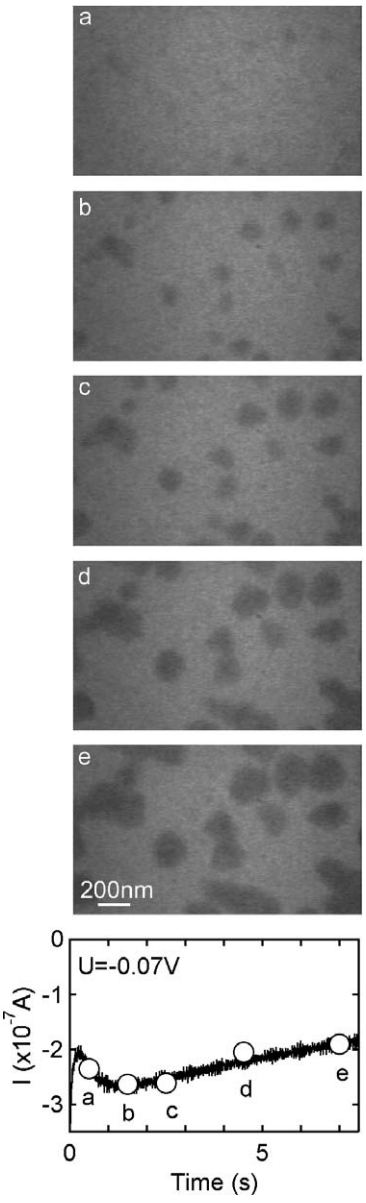

Fig. 7. A sequence of images recorded simultaneously with deposition at −0.07 V.

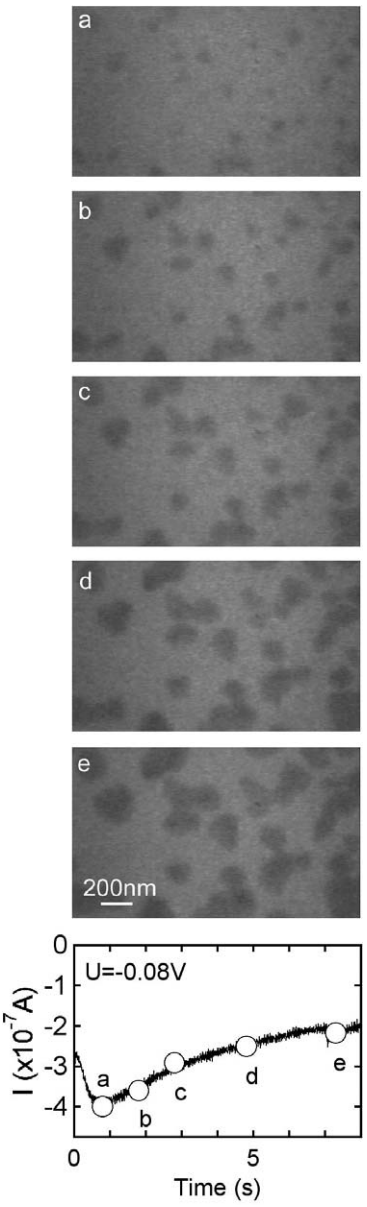

Fig. 8. A sequence of images recorded simultaneously with deposition at −0.08 V.

and they are not as strongly faceted as at −0.05 V. At longer times the islands continue to grow and the island on the left coalesces with another island. The time at which the current transient reaches its maximum value (t_{max}) occurs at about 8 s, considerably shorter than the value of 15 s for the deposition transient at −0.05 V.

At more negative potentials from −0.07 V (Fig. 7) to −0.10 V (Fig. 10) islands appear as soon as the potential reaches its nominal value. In other words, the *induction time*, i.e., the time before any islands become visible, decreases to values less than the video capture rate (1/30 s). In this potential range, deposition is diffusion limited. The time t_{max} at which the transients reach their maximum current values becomes shorter, and the value of the current at this maximum becomes larger. The images show that in this diffusion limited regime the islands (in projection) are not faceted but are almost circular, as expected. In each experiment, the island density increases with time, and by comparing Figs. 7–10 we see that the final island density increases as the deposition potential becomes more negative.

The area of the field of view in the TEM is 2.64 μm^2, about 760 times smaller than the total electrode area. Before analysing the data shown above, it is important to determine whether the images in the field of view are representative of the total electrode area. To examine this we compare the charge associated with the islands in the field of view with the charge transferred over the whole electrode area.

The charge density associated with the whole electrode is easily obtained by integrating the current transients and

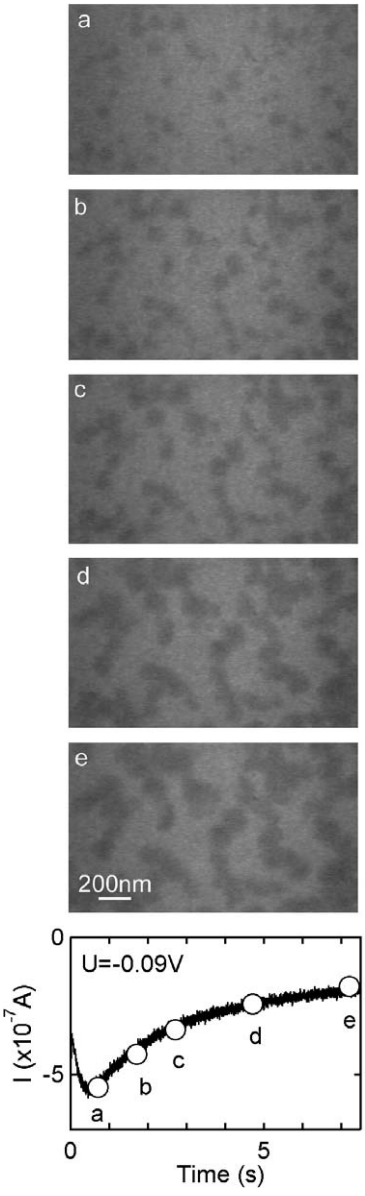

Fig. 9. A sequence of images recorded simultaneously with deposition at −0.09 V.

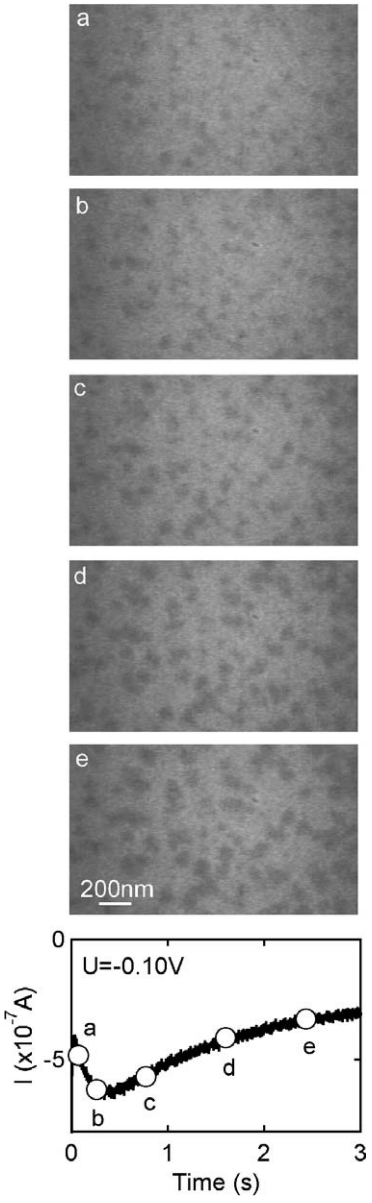

Fig. 10. A sequence of images recorded simultaneously with deposition at −0.1 V.

dividing by the total electrode area. The charge density associated with the copper islands in the images is obtained from Faraday's law:

$$q_{\text{total}} = \frac{1}{S}\sum_{i=1}^{N} Q_i = \frac{1}{S}\sum_{i=1}^{N} \frac{zF}{V_{\text{m}}} V_i \qquad (2)$$

where V_{m} is the molar volume of copper (7.1 $\text{cm}^3\,\text{mol}^{-1}$), $V_i = 2\pi r_{\text{eff}}^3/3$ is the volume of the ith island, $z = 2$ is the charge on the ion, F is Faraday's constant, and r_{eff} is the effective island radius. The summation is performed over N islands not touching the frame edge. The area S for the calculation is the area of the field of view minus a buffer area around the perimeter of the image with width equal to diameter of the largest island in contact with the frame edge. In the calculation we assume that all islands are hemispherical. Post-growth AFM analysis shows that this is a reasonable assumption, although a small fraction of islands are spherical segments with height less than the base radius.

Fig. 11 shows the charge density obtained from the images and from the transients for deposition at −0.08 V. The two curves show excellent agreement up to 3 s, well beyond the time corresponding to the current peak (3 s $\approx 4t_{\text{max}}$), i.e., beyond the point where the diffusion fields for individual islands begin to interact. At longer times, the slight deviation between the two curves is due to island coalescence. In the analysis of the images, the projected area of two islands that are touching is divided between the two islands and the effective radius of each island calculated from the area. This calculation underestimates the total volume in clusters that have coalesced resulting in the slight

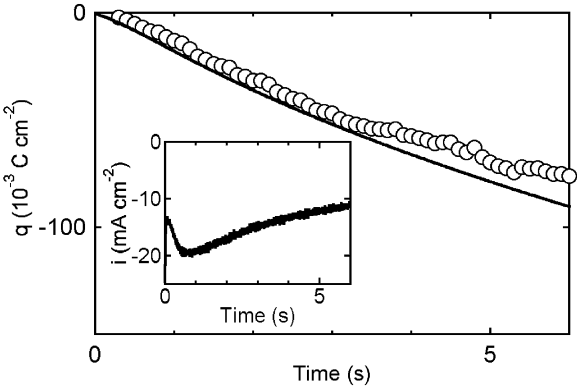

Fig. 11. Comparison of microscopic (derived from images) and macroscopic (derived from total current) charge density transients for copper deposition on gold at −0.08 V. (Solid line) integration of the deposition current transient (shown in the inset) and (○) charge obtained from images using Eq. (2).

deviation at longer times. Thus these results clearly show that the field of view in the TEM is representative of the whole electrode area, and allow us to make quantitative comparisons between the island kinetics observed in the images and the kinetics deduced from the transients.

4.3. Island nucleation kinetics

It is straightforward to measure the number of islands in each frame of a video, and hence determine directly the nucleation kinetics for each potential. Fig. 12 shows the time evolution of the island density for deposition potentials from −0.06 V to −0.09 V. Also shown in the figures are curve fits assuming first order nucleation kinetics:

$$N(t) = N_0(1 - \exp(k_n t)) \quad (3)$$

where $N(t)$ is the time-dependent island density, N_0 is the saturation island density at sufficiently long times, and k_n is the nucleation rate constant. Analysis was not possible at −0.05 V and −0.10 V; at −0.05 V only one island was observed in the field of view and at −0.10 V the island density saturated in the first two frames. For the intermediate potentials, Eq. (3) provides a good fit to the experimental data, indicating that nucleation can be described very well by first order kinetics and a nucleation rate constant, k_n. The values of N_0 and k_n derived from these curve fits are shown in Fig. 13. These results represent one of the first direct measurements of island density as a function of time and provide insight into the kinetics of nucleation in electrodeposition. Measurements using ex situ scanning probe microscopy or scanning electron microscopy [18–20] are limited by the fact that each measurement of $N(t)$ requires a different sample.

The time evolution of the island density expressed in Eq. (3) has two limiting cases. For $k_n t > 1$ (instantaneous nucleation) the exponential term is negligible and $N(t) = N_0$ at all times, whereas for $k_n t < 1$, the exponential term can be linearized and we obtain $N(t) = k_n N_0 t$ for small times (progressive nucleation). At the time corresponding to the current maximum in the deposition transients, t_{max}, the values for $k_n t$ are about 10–12 and hence from Eq. (3) we can see that the island density is close to saturation ($N(t) \approx N_0$). The condition $k_n t < 1$ is satisfied only when $t < 0.1 t_{max}$ illustrating that the nucleation kinetics for the experimental conditions reported here are intermediate between the two limiting cases. It therefore appears necessary to include the complete first order equation (Eq. (3)) in any analysis, rather than assuming either of the limiting cases, as has often been done to simplify analysis.

The saturation island density N_0 increases from 1.9×10^8 cm^{-2} at −0.06 V to 4.3×10^9 cm^{-2} at −0.10 V. Note that the single island seen at −0.05 V corresponds to an upper limit in the island density of 3.8×10^7 cm^{-2}. For the potentials where deposition is diffusion limited (−0.07 V to −0.10 V) the island density increases exponentially with an inverse slope of 47 mV per decade, somewhat smaller than values obtained for copper deposition on Si (99 mV per decade) [5], TiN (140 mV per decade) [4], and TaN (150–250 mV per decade) [6]. The slope provides useful information on the ability to change the island density by varying the deposition overpotential; a lower slope indi-

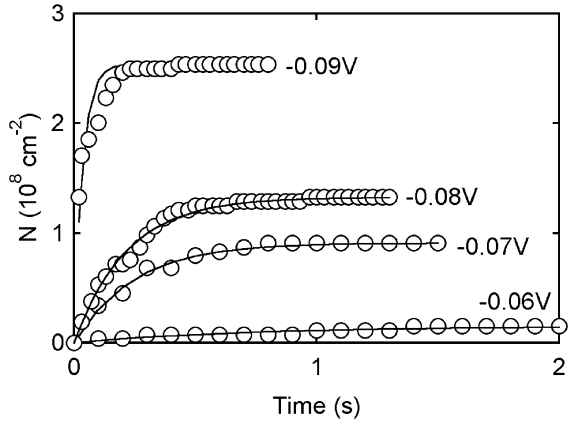

Fig. 12. Time evolution of the island density for deposition at −0.06 V, −0.07 V, −0.08 V, and −0.09 V.

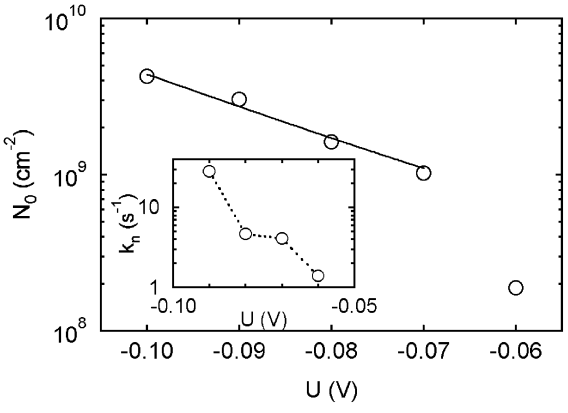

Fig. 13. Potential dependence of island density (N_0), and (inset) nucleation rate constant (k_n) obtained from Fig. 12.

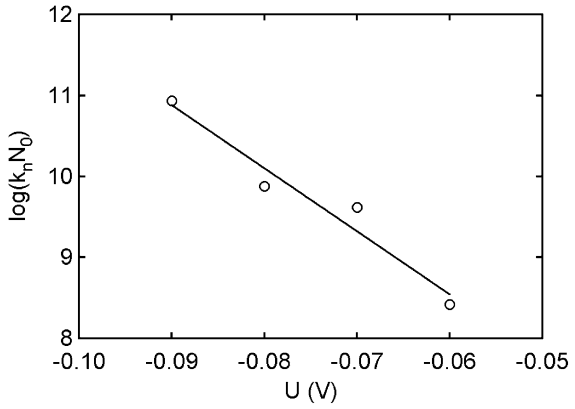

Fig. 14. Potential dependence of the nucleation rate (k_nN_0), fitted by a straight line from which the critical nucleus size can be derived.

cates that a larger overpotential is needed to give a desired increase in island density.

The inset to Fig. 13 shows that the nucleation rate constant k_n increases approximately exponentially with potential from 1.4 s^{-1} at −0.06 V to 28.4 s^{-1} at −0.09 V. Fig. 14 shows the product k_nN_0 plotted versus the deposition potential. The inverse slope of 13 mV per decade is smaller than the slopes obtained for copper deposition on Si (45–89 mV per decade) [5,20]. From classical electrocrystallization theory [21], the critical nucleus size, n_{crit}, can be obtained from the potential dependence of the nucleation rate:

$$\frac{\mathrm{d}\log(k_nN_0)}{\mathrm{d}|U|} = \frac{e}{2.303\mathrm{kT}}(\beta + n_{crit}) \quad (4)$$

where η is overpotential, and β is a parameter with a value between 0 and 1 depending on the attachment mode. Taking $\mathrm{d}|U|/\mathrm{d}\log k_nN_0 = 0.013$ V we obtain a critical nucleus size $n_{crit} = 3$, in excellent agreement with the findings of Holzle et al. [1]. It is interesting that our value, obtained by analysis of the nucleation kinetics recorded directly for an ensemble of islands, is identical to the value obtained by scanning probe microscopy of the earliest stages of growth during underpotential deposition. The small critical nucleus size suggests that atom de-attachment from the islands, resulting in the generation of adatoms on the surface or ions in solution, is very slow.

5. Summary

Historically, analysis of island growth during bulk (overpotential) deposition has relied on the recording of current transients at different deposition potentials which are then fitted using various analytical growth models. Since the analytical models are based on various assumptions and hence restricted to a limited set of conditions, the ability to image the surface simultaneously with electrochemical measurement provides a powerful tool to explore the details of island growth in electrodeposition. In part due to the difficulty in imaging bulk electrodeposition, the parameters that control island growth are not well understood.

Here we have demonstrated that parameters such as the island shape, density and nucleation rate can be measured directly. In terms of the island shape, we see a gradual transition from faceted to circular islands as we change the deposition potential from conditions at which the surface reaction (or a mixed process) is expected to be rate limiting to conditions where bulk diffusion is rate limiting. As we change potential, we also see systematic trends in the final island density and the initial nucleation rate. Simple analysis of the density of islands as a function of time verify directly one key assumption made in growth models, that nucleation kinetics are first order, but shows that for a range of potentials it is not sufficient to take one of the limiting cases often assumed for nucleation kinetics, i.e., progressive or instantaneous nucleation. Finally, we have shown that these direct measurements of the variation of rate constant and nucleus density as a function of potential can be used to derive a value for the critical nucleus size that is in agreement with the value derived from other techniques.

It is clear that a technique combining real-time imaging and electrochemical measurements can provide a great deal of information on the electrochemical nucleation and growth process. As well as the measurement of collective properties such as island density as a function of time, it is also possible to measure the growth kinetics of individual islands. Initial results show that these measurements also confirm some of the rate laws expected from diffusion limited growth models, but demonstrate significant discrepancies in some key parameters. The further analysis of such quantitative data provides a starting point for testing and improving electrochemical growth models, with the ultimate aim of understanding electrochemical process in enough detail to predict and design the microstructure of electrodeposited materials.

Acknowledgements

We gratefully acknowledge financial help from IBM through IBM Faculty Award and IBM Graduate Student Summer Internship, and the Johns Hopkins University MRSEC (NSF grant number DMR05-20491). We acknowledge the invaluable help of M.C. Reuter, A. Ellis and S.J. Chey in the experimental aspect of this work and R.M. Tromp and M.J. Williamson for useful discussions.

References

[1] M.H. Holzle, C.W. Apsel, T. Will, D.M. Kolb, Journal of the Electrochemical Society 142 (1995) 3741.
[2] M.H. Holzle, V. Zwing, D.M. Kolb, Electrochimica Acta 40 (1995) 1237.
[3] P.M. Vereecken, K. Strubbe, W.P. Gomes, Journal of Electroanalytical Chemistry 433 (1997) 19.
[4] A. Radisic, J.G. Long, P.M. Hoffmann, P.C. Searson, Journal of the Electrochemical Society 148 (2001) C41.

[5] A. Radisic, A.C. West, P.C. Searson, Journal of the Electrochemical Society 149 (2002) C94.
[6] A. Radisic, Y. Cao, P. Taephaisitphongse, A.C. West, P.C. Searson, Journal of the Electrochemical Society 150 (2003) C362.
[7] O. Chyan, T.N. Arunagiri, T. Ponnuswamy, Journal of the Electrochemical Society 150 (2003) C347.
[8] G. Gunawardena, G. Hills, I. Montenegro, B. Scharifker, Journal of Electroanalytical Chemistry 138 (1982) 225.
[9] B. Scharifker, G. Hills, Electrochimica Acta 28 (1983) 879.
[10] J.J. Kelly, C.Y. Tian, A.C. West, Journal of the Electrochemical Society 146 (1999) 2540.
[11] J.P. Healy, D. Pletcher, M. Goodenough, Journal of Electroanalytical Chemistry 338 (1992) 155.
[12] W. Plieth, Electrochimica Acta 37 (1992) 2115.
[13] M.J. Williamson, R.M. Tromp, P.M. Vereecken, R. Hull, F.M. Ross, Nature Materials 2 (2003) 532.
[14] F.M. Ross, A. Radisic, M.J. Williamson, S.J. Chey, R.M. Tromp, M.C. Reuter, A. Ellis, R. Hull, and P.C. Searson, in preparation.
[15] A. Radisic, P.M. Vereecken, J.B. Hannon, P.C. Searson, F.M. Ross, Nano Letters 6 (2006) 238.
[16] A.J. Bard, L.R. Faulkner, Electrochemical Methods: Fundamentals and Applications, John Wiley, New York, 2001.
[17] T.I. Quickenden, Q.Z. Xu, Journal of the Electrochemical Society 143 (1996) 1248.
[18] C. Ji, G. Oskam, P.C. Searson, Journal of the Electrochemical Society 148 (2001) C746.
[19] C.X. Ji, G. Oskam, P.C. Searson, Surface Science 492 (2001) 115.
[20] P.M. Hoffmann, A. Radisic, P.C. Searson, Journal of the Electrochemical Society 147 (2000) 2576.
[21] E. Budevski, G. Staikov, W.J. Lorenz, Electrochemical Phase Formation and Growth, VCH, New York, 1996.